

A preliminary study on the knowledge-based delineation of anatomical structures for whole body PET-CT Studies

Lingfeng Wen, *Member, IEEE*, Wilson Leung, Stefan Eberl, *Member, IEEE*,
Dagan Feng, *Fellow, IEEE*, Jing Bai, *Fellow, IEEE*

Abstract— PET-CT imaging has shown its superiority in the clinical management of cancer. The markedly increased amount of imaging data have given rise to the development of computer-aided diagnosis (CAD) to aid the clinician in the interpretation of large volumes of data. The delineation of anatomical structures is one of the major components of CAD. Currently, the majority of segmentation methods are focused on the segmentation of organs and tissues using high-contrast anatomical images such as high-dose CT with injected contrast agent. However, typically low-dose CT protocol without the use of contrast agent are used in PET-CT studies, which leads to low-contrast CT images with a relatively high level of noise. This study investigated the potential of using information extracted from the co-registered PET-CT data in the segmentation of anatomical structures. A preliminary knowledge-based system was developed to process eight clinical PET-CT studies for lung cancer. The results of qualitative and quantitative analysis demonstrate the efficiency of incorporating the information derived from co-registered structural and functional images in the segmentation of anatomical structures for whole body PET-CT studies. It also implies that the methods relying on the HU value, like thresholding, are incapable of accurately delineating those organs suffering from high-level noise with unclear boundary. Further investigation using advanced technologies are warranted to achieve accurate segmentation for PET-CT imaging.

I. INTRODUCTION

PET-CT is a relatively new imaging technology which combines positron emission tomography (PET) and fast multi-slice helical X-ray computed tomography (CT) in the one instrument [1]. PET images provide biochemical and physiological information, while CT images provide structural details, improving image quality of PET by CT-based attenuation correction. The combination of

anatomical and functional images has demonstrated its great benefits in tumor detection, staging and the evaluation of treatment response in the management of cancer [2]. Unlike other diseases, cancer is not necessarily only limited to one primary organ, but also may involve local and distant metastases to the lymphatic system and other organs [3].

The diagnostic process requires experts to read a large amount of images, interpreting abnormalities with prior knowledge about anatomical structures and determining the stage of cancer, which is essential for determining the most appropriate treatment. However, even for experienced clinicians, it is challenging to efficiently review this large volume of data and the ever increasing volumes of data increase the likelihood of missing abnormalities.

Computer-aided diagnosis (CAD) schemes have the potential to improve diagnostic performance by detecting malignant lesions and delineating anatomical structures [4]. The current developments in segmentation are mainly focused on delineating organs and tissues using high-contrast structural images like CT [5-7]. There are many diverse approaches for segmentation like region growing, clustering, watershed transform, deformable model and graph theory. However, to minimise radiation dose, PET-CT scans usually employ low-dose CT protocols without the use of injected contrast agent. These protocols result in low-contrast CT images with less clearly defined organ boundaries and high-level statistical noise.

PET images readily allow identification of organs like the brain due to high metabolism, while CT images are most suitable for extracting the areas of the lungs and the skeleton due to their distinctly differences in density compared to soft tissue. Despite of this, there is a paucity of research extracting and utilizing the complementary information offered by PET and CT in segmentation. Thus, in this paper, we investigated the potential of using the information extracted from co-registered PET-CT imaging in structure delineation for whole body studies by using a knowledge-based system to process clinical data.

II. METHODS

A. Knowledge-based system for whole body segmentation

Fig. 1 shows a flowchart of the proposed knowledge-based system, which consists of several components: pre-processing with bed removal; delineation of brain and bladder from PET data; extracting spine and respiratory area

Manuscript received February 29, 2008. This work was supported in part by ARC, PolyU/UGC grants, and ISL/Australia-China special fund.

Dr Lingfeng Wen and Prof Dagan Feng are with the Biomedical and Multimedia Information Technology (BMIT) Research Group, the School of Information Technologies, University of Sydney, Australia. They are also with the Department of Electronic and Information Engineering, Hong Kong Polytechnic University, Hong Kong. (e-mail: wenlf@ieee.org; feng@it.usyd.edu.au).

Mr Wilson Leung was with the School of Electrical and Information Engineering, University of Sydney, Australia (e-mail: wleung01@gmail.com).

A/Prof Stefan Eberl is with the Department of PET and Nuclear Medicine, Royal Prince Alfred Hospital, Sydney, Australia. He is also with the School of Information Technologies, University of Sydney, Australia (e-mail: stefan@cs.usyd.edu.au).

Prof Jing Bai is with the Department of Biomedical Engineering, Tsinghua University, Beijing 100084, China. (e-mail: deabj@mail.tsinghua.edu.cn)

from CT data; segmenting liver and kidney using PET-CT data.

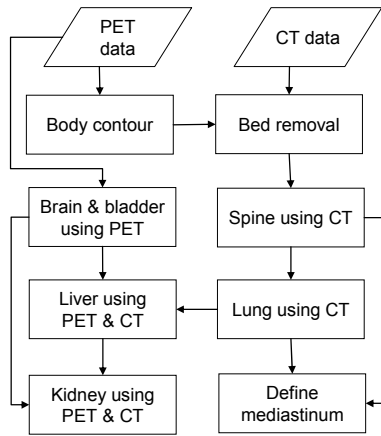


Fig. 1. The data flow of the proposed delineation method

1) *Preprocessing*: The patient bed shows a density similar to body tissues in CT images, which may increase computational cost in the processing of data. Instead of using a template of the patient bed derived from a blank scan, we developed a general approach to use individual information from the functional images to remove the bed in the structural images.

The tracer uptake in the PET images is firstly converted to standard uptake values (SUV) by normalization the uptake with the injected dose and the body weight of the patient to reduce inter-patient variability [8]. A low value is used to threshold SUV images to obtain the body contour, which is then transformed to the CT images for isolating the bed.

2) *High FDG uptake organs*: The brain, as glucose is its main energy source, has high uptake of FDG in the high metabolism cortices. FDG is excreted through the kidneys resulting in a high concentration of FDG in the bladder. Thus these two landmark structures are easily identifiable on the PET images to identify the brain and abdominal regions.

The whole body SUV images are thresholded at half the global maximum SUV pixel value to extract high FDG uptake tissues, followed by the region growing to derive candidate volumes. These candidate volumes will include the brain and bladder as well as potentially tumors, which also have high FDG uptake. The largest volume is labeled as the brain, while the bladder was defined as the second largest volume crossing the central line of the sagittal view at the opposite end of the scan range to that of the brain.

3) *Spine*: The spine, an aggregate of vertebrae extending from the skull to the pelvis, can be used as a reference landmark in the anatomical localization. The contiguous characteristic of the vertebrae in the spine allows it to be segmented progressively from a defined starting point using the 2D transverse images. The CT images are in Hounsfield Units (HU), representing the relative attenuation of the tissue with respect to water and air. By using the HU range of bone,

most bone tissues can be segmented from the CT images. We then apply a region continuity method to derive the spine.

A 2D delineation of the spine is firstly derived based on its known anatomical location relative to the bladder on a transverse image containing the segmented bladder. Starting from the initial plane, the spine with partial inclusion of ribs will be determined in the next plane by choosing the largest 2D region, which has the most overlapped regions with the definition of spine on the previous plane. For the simplicity, the searching is confined to the planes extending from the base of the brain and to the bottom of the bladder.

4) *Lung and trachea*: While the lung has characteristically low HU values, it is not just a simple matter of thresholding to derive the lungs. Thresholding will also extract the trachea, and air pockets in the stomach and gastro intestinal tract and these pose a challenge in delineating the lungs.

Firstly, a rough thoracic region is defined based on the locations of the brain and bladder. An initial seed is then selected from the thresholded CT images for the HU range of lungs by using a rule-based approach in terms of the spine, followed by region growing to derive the regions of the lung with the trachea using two constraints in HU value of pixels: the maximum allowable difference to the initial seed (ΔHU_S) is 600, and the maximum difference between the adjacent pixels (ΔHU_A) is 200.

A narrower HU range with ΔHU_S of 80 and ΔHU_A of 40 is then used in region growing to derive the rough estimation of the trachea with the binary dilation technique, which is applied to generate a larger image mask for searching all the trachea pixels. Once the trachea is segmented, a 3D pixel-wise subtraction [9] is applied to generate the delineation of the lung.

5) *Liver*: Being different from the lung and spine, the liver lacks a clear boundary in these low-contrast CT images. The slightly higher SUV values in the PET images are not sufficient to achieve the segmentation of the liver. Thus, we attempted to segment the liver using an integrated information-based adaptive approach with the information extracted from co-registered PET and CT images.

A binary mask image, A , is firstly derived to cover the liver with partial inclusion of adjacent organs using a relative HU range for the liver on the transverse images confined between the locations of the lung and the bladder. An adaptive technique is then applied to search for the optimal lower bound for thresholding the liver using the PET data with the binary mask image B by maximizing the objective function Φ (1),

$$\Phi = \max[N(A \wedge B) - N(\neg A \wedge B)] \quad (1)$$

where N is the total number of non-zero pixels, \wedge is the logic operator of AND, \neg is the logic operator of NOT. Finally the liver is segmented by combining B and a new binary mask image from the CT data using the specific HU range of the liver.

6) *Kidneys*: The kidneys have a symmetric spatial location relative to the spine. Thus two initial seeds will be obtained in

PET images by comparing the regions of high SUV with corresponding spatial locations. Region growing is then performed in CT image to derive a rough segmentation of the two kidneys. An adaptive procedure similar to that used for the liver is then applied to segment the two kidneys.

7) *Mediastinum*: The mediastinum is an area in the thoracic cavity bounded by the two pleural sacs, the sternum anteriorly and the vertebral column posteriorly. We apply a simple method to draw a boundary defined by the spine and medial edges of the lungs on the transverse images.

B. Clinical data

The clinical data were obtained with a Siemens Biograph Duo PET-CT scanner with multiple bed positions to cover the body from the head to the pelvis. Any mismatch between the PET and CT data was corrected by the co-registration software of the vendor on an on-site workstation, resulting in the images with the matrix size of 512 by 512 pixels (pixel size: 1.0 mm).

There are eight PET-CT studies (4 males: 67±8 yo, 3 females: 64±7 yo) extracted from the hospital archive system. All the patients have been diagnosed with non-small cell lung cancer (NSCLC) with stages ranging from stage I to stage IV.

C. System implementation

Considering the aim of this paper, the PET-CT images were rescaled to images with 256 by 256 pixels (pixel size: 2.0 mm), using a bilinear interpolation in order to reduce computational cost.

The system was implemented using the Java Software Development Kit and Matlab package (version: 7.0.1) on a laptop with a 2.0 GHz CPU and 1 GB memory.

D. Qualitative analysis of reliability

The software package of OpenDX [10] is used to visualize the labeled structures through 3D rendering (Fig.2). The reliability in segmenting each structure was evaluated by visual inspection.

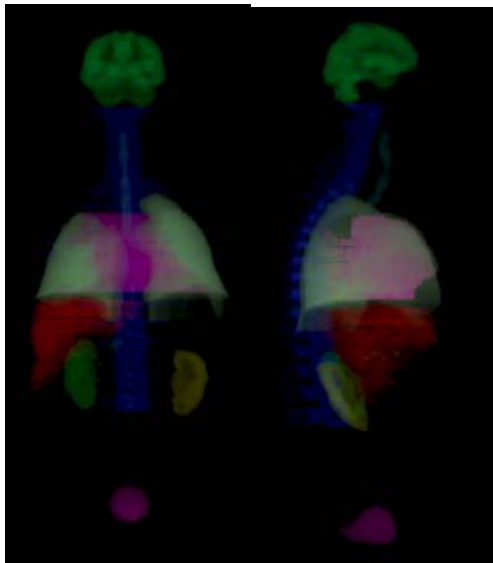


Fig.2. The coronal view (left) and sagittal view (right) of the obtained structure delineation of one PET-CT study

The reliability of structure delineation is scored as “OK” if the boundaries were correctly extracted, “Poor” when the structures were identified, but boundary definition was inaccurate or “Failed” when a structure failed to be identified and extracted.

E. Quantitative analysis of accuracy

The accuracy of the knowledge-based segmentation was evaluated by a quantitative similarity measure compared to the manual segmentation outcomes of a human operator.

C is the binary image mask derived from the automated system while D is the binary image mask from the manual delineation. Three parameters were derived: the accuracy ratio (2), under-segmentation ratio (3) and over-segmentation ratio (4).

$$Acu = N(C \wedge D) / N(D) \times 100\% \quad (2)$$

$$Und = N(\neg C \wedge D) / N(D) \times 100\% \quad (3)$$

$$Ovr = N(C \wedge \neg D) / N(D) \times 100\% \quad (4)$$

For perfect segmentation, Acu is equal to 100% with Und and Ovr being 0%.

III. RESULTS

A. Reliability

The reliability of the segmentation is listed in Table I. It is not entirely surprising that the method is not capable of processing all clinical data due to the simplicity of the developed system for the challenging low-contrast PET-CT data. The results show that the cancerous lesions of NSCLC didn't distract the structure delineation if the lesion was not attached to the boundary of one of the structures.

Table I. Reliability of the structure delineation

ID	Brain	Bladder	Spine	Lung	Liver	Kidney	Med [*]
P1	OK	OK	OK	OK	OK	OK	OK
P2	OK	OK	OK	OK	Poor	Poor	OK
P3	OK	OK	OK	Failed	OK	Poor	Failed
P4	OK	OK	OK	OK	OK	OK	OK
P5	OK	OK	OK	OK	OK	Poor	OK
P6	OK	OK	OK	OK	Failed	Failed	Failed
P7	OK	OK	OK	OK	OK	Poor	OK
P8	OK	OK	OK	OK	Poor	Poor	OK

* Med: Mediastinum

The possible reasons of the poor and failed delineation were found to be as follows, by interpreting the original PET/CT data.

P2, P5, P8: The CT images suffer from noise, causing the HU values of some pixels to fall outside the normal range.

P3: Invading tumors caused the thinned delineation of the right bronchi, leading to the failed detection of the right lung.

P6: Liver FDG uptake was the highest in the abdomen, causing the failed detection of the right kidney.

B. Quantitative similarity

Table II lists the quantitative accuracy for one study.

Table II. Similarity measures of the segmentation for P1

%	Brain	Bladder	Spine	Lung	Liver	Kidney	Med [*]
<i>Acu</i>	95.3	96.2	94.7	96.6	33.6	38.4	96.2
<i>Und</i>	4.7	3.8	5.3	3.4	66.4	61.6	3.8
<i>Ovr</i>	0.1	7.2	69.9	0.3	0.0	0.1	2.9

* Med: Mediastinum

The results demonstrate reasonable delineations were achieved for the brain, bladder and lung with slight misclassification of some voxels (*Und* and *Ovr*) due to partial volume effect in PET imaging and inappropriate SUV for thresholding. The over-segmentation of the spine with $Ovr=69.9\%$ is not unexpected as the current continuity method doesn't apply sufficient constraints to remove the merging area between the ribs and vertebrae.

Unexpectedly, severe under-segmentations were observed for the liver and the kidney. This is mainly because of the lack of clear organ boundaries in the low-contrast CT images, which cause the thresholding technique to be insufficient to clearly label and delineate these organs. Despite of reasonable segmentation of the mediastinum achieved for P1, under-segmentation was also observed for other studies due to the asymmetry in the thoracic area. These findings imply that the methods relying on the HU value, like thresholding, are incapable of accurately delineating those organs suffering from high-level noise and hence ill-defined boundaries.

C. Computational cost

Table III lists the computational time for each component. For all the successful delineation, the total running time is about 3 minutes.

Table III. The running time (seconds) for each structure

ID	Brain	Bladder	Spine	Lung	Liver	Kidney	Med [*]
P1	1.6	1.7	29	31	58	24	26
P2	1.8	1.5	26	27	65	16	27
P3	1.5	1.7	22	--	56	35	--
P4	1.6	1.7	23	31	71	22	25
P5	1.3	1.5	25	29	69	32	23
P6	1.3	1.8	21	20	--	--	--
P7	1.3	1.5	22	23	53	22	22
P8	1.5	1.7	27	30	59	27	27

* Med: Mediastinum

IV. CONCLUSION

This preliminary study investigated the potential use of information extracted from the co-registered PET-CT data in the segmentation of anatomical structures. The results demonstrate the efficiency of incorporating multi-modality information derived from co-registered structural and functional images with anatomical knowledge. It also implies that the methods relying on the HU value, like thresholding, are incapable of accurately delineating those organs suffering from high-level noise and thus ill-defined boundaries. Further investigation will be warranted to achieve accurate segmentation for PET-CT imaging using advanced technologies such as wavelet transform [11] and morphological analysis [12].

REFERENCES

- [1] T. Beyer, D. W. Townsend, T. Brun, et al., "A combined PET/CT scanner for clinical oncology," *Journal of Nuclear Medicine*, vol. 41, pp. 1369-1379, 2000.
- [2] B. M. Fischer and J. Mortensen, "The future in diagnosis and staging of lung cancer: Positron emission tomography," *Respiration*, vol. 73, pp. 267-276, 2006.
- [3] U. W. Knoepp and J. G. Ravenel, "CT and PET imaging in non-small cell lung cancer," *Critical Reviews in Oncology Hematology*, vol. 58, pp. 15-30, 2006.
- [4] I. Sluimer, A. Schilham, M. Prokop, et al., "Computer analysis of computed tomography scans of the lung: A survey," *IEEE Transactions on Medical Imaging*, vol. 25, pp. 385-405, 2006.
- [5] L. Zhang, E. A. Hoffman, and J. M. Reinhardt, "Atlas-driven lung lobe segmentation in volumetric X-ray CT images," *IEEE Transactions on Medical Imaging*, vol. 25, pp. 1-16, 2006.
- [6] I. Sluimer, M. Prokop, and B. Van Ginneken, "Toward automated segmentation of the pathological lung in CT," *IEEE Transactions on Medical Imaging*, vol. 24, pp. 1025-1038, 2005.
- [7] S. Y. Hu, E. A. Hoffman, and J. M. Reinhardt, "Automatic lung segmentation for accurate quantitation of volumetric X-ray CT images," *IEEE Transactions on Medical Imaging*, vol. 20, pp. 490-498, 2001.
- [8] D. Feng, L. Wen, and S. Eberl, "Techniques for Parametric Imaging," in *Biomedical Information Technology*, D. Feng, Ed. San Diego: Elsevier press, 2007, pp. 137-163.
- [9] R. C. Gonzalez and R. E. Woods, "Dilation and Erosion," in *Digital Image Processing*, 2 ed. New Jersey: Prentice-Hall, 2002, pp. 523-527.
- [10] D. Thompson, J. Braun, and R. Ford, *OpenDX: Paths to Visualization*. VIS Inc., 2000.
- [11] O. Talakoub, J. Alirezaie, and P. Babyn, "Lung Segmentation in Pulmonary CT Images using Wavelet Transform," presented at *IEEE International Conference on Acoustics, Speech and Signal Processing*, 2007.
- [12] M.-E. Lee, S.-H. Kim, S.-W. Kim, et al., "Automatic Segmentation Methods for Various CT Images Using Morphology Operation and Statistical Technique," presented at *IEEE International Conference on Intelligent Computer Communication and Processing*, 2007.